Composites Part A **111** (2018) 106–114

Doi: 10.1016/j.compositesa.2018.05.013

Viscoelastically prestressed polymeric matrix composites: An investigation into fibre deformation and prestress mechanisms

Bing Wang [a,b], Kevin S. Fancey [a*]

[a] GW Gray Centre for Advanced Materials, School of Engineering & Computer Science, University of Hull, HU6 7RX, UK
[b] Department of Engineering, University of Cambridge, CB2 1PZ, UK

Abstract

A viscoelastically prestressed polymeric matrix composite (VPPMC) is produced by subjecting polymeric fibres to a creep load, which is removed before moulding the fibres into a polymeric matrix. The resulting fibre viscoelastic recovery creates compressive stresses within the cured matrix. Although mechanical properties can be improved by up to 50%, the effect of fibre creep stress magnitude on VPPMC performance is unknown. In this paper, viscoelastic effects were investigated for 24 h creep stress values of 330-590 MPa. This involved recovery force measurement and wide-angle X-ray diffraction (WAXD) on nylon 6,6 fibres and Charpy impact testing of nylon fibre-polyester resin VPPMCs. Greatest performance was achieved with an intermediate value (460 MPa), suggesting an optimum creep stress condition. Moreover, with increasing creep stress, WAXD demonstrated a progressive reduction in regions with viscoelastic energy storage capability. By considering polymeric three-phase microstructural and latch-based mechanical models, a viscoelastic fibre-generated prestress mechanism is proposed.

Keywords: A. Polymer-matrix composites (PMCs); B. Impact behaviour; B. Residual/internal stress; Viscoelasticity.

[*] Corresponding author. Tel.: + 44 1482 465071; fax: +44 1482 466664.
E-mail address: k.s.fancey@hull.ac.uk (K.S. Fancey).

1. Introduction

To produce a polymeric matrix composite (PMC), substantial residual stresses can be developed during manufacture. These stresses are generated from (i) shrinkage of the polymeric matrix during curing, and (ii) thermal expansion mismatch between fibre and matrix materials [1,2]. Although residual stresses can occasionally be beneficial, they are usually detrimental [3]. Depending on fibre-matrix combinations and laminate stacking sequences, the accumulation of residual stresses can lead to fibre waviness [4], laminate warping, buckling or matrix cracking [5]. Therefore, these stresses can significantly affect the mechanical performance of composite products, or even lead to premature fracture of a composite structure [1]. Prestressed PMCs were first developed to counteract these residual stresses from manufacture. Zhigun [6] and Tuttle [7] were amongst the earliest investigators, exploiting the principles used in prestressed concrete production. These elastically prestressed PMCs (EPPMCs) are produced by applying tension to fibres embedded in uncured resin, the tensile load being released after resin curing. Owing to attempted elastic recovery by residual fibre tension, a compressive stress is generated within the resin matrix, which can improve the composite mechanical properties [8-21].

For polymeric fibres, an applied tension can cause elastic (instantaneous) strain and viscoelastic (time-dependent) creep strain; then removing the tension leads to elastic recovery, followed by viscoelastic recovery. Thus prestressed composites can also be produced by exploiting viscoelastic recovery, i.e. viscoelastically prestressed PMCs (VPPMCs) [22,23]. Here, tension is applied to polymeric fibres, then the tensile load is released before moulding the fibres into a matrix. Following matrix curing, viscoelastic recovery mechanisms within the fibres create compressive stresses in the matrix, counterbalanced by fibre tension. For nylon fibre-based VPPMCs, viscoelastically generated prestress has been shown to improve tensile strength by ~15% [24], impact toughness by 30-60% [25-29], and flexural stiffness by ~50% [30,31].

Though both methods can provide similar mechanical property improvements, there are notable advantages to VPPMCs over EPPMCs [25,28,32]. Since fibre prestressing and moulding processes are decoupled for VPPMC production, there is total flexibility in terms of product shape and size; this is in contrast with EPPMC production, where the tensile load must be maintained throughout the matrix curing process, potentially restricting product geometry [25]. Also, equipment designs for simultaneous stretching and moulding can be technically challenging [16,33]. A further advantage of VPPMCs is their longevity. Elastically generated prestress can be expected to deteriorate with time and, to some extent, this has been observed by Mostafa *et al* [20]. The deterioration occurs through the prestress causing localised matrix creep at the fibre-matrix interface regions. In VPPMCs however, any potential for this matrix creep would be offset by longer term viscoelastic recovery mechanisms within the fibres [25]. Thus although viscoelastic activity is temperature-sensitive, nylon fibre-based VPPMC samples subjected to accelerated aging (using time-temperature superposition) have demonstrated no deterioration in increased impact energy absorption over a duration equivalent to ~25 years at 50°C ambient [28]. For further information on the fundamental aspects of VPPMC materials, we refer the reader to a recently published review [32].

For VPPMC production, a creep condition of 320-340 MPa applied for 24 h has been used for the majority of investigations into nylon 6,6 fibre-based VPPMCs [24,26-31,34-37]. Recent work however, has demonstrated that the creep processing time could be significantly reduced from 24 h to tens of minutes by using higher creep stress values, with no detriment to improved mechanical (Charpy impact) performance [29]. In addition to mechanical property improvements, viscoelastic fibre prestressing can be used to produce morphing (bistable) structures [36,37]. For example, a pair of deflecting VPPMC strips can be bonded on each side of a thin, flexible resin-impregnated fibre-glass sheet to generate opposite out-of-plane deflections [37]. Thus, the structure is stable in two cylindrical shapes with opposing states of curvature, so that it can readily "snap" between these two states. Such structures may open new opportunities for VPPMC technology; e.g. control surfaces for aerospace applications.

Clearly, the benefits from prestress within a VPPMC are determined by the time-dependent viscoelastic recovery of polymeric fibres; however, the effect of creep stress magnitude on the resulting mechanical performance of VPPMCs is still unknown. In this paper, we have applied a range of creep stress conditions to nylon 6,6 yarns, to produce VPPMC samples for subsequent Charpy impact testing. Here,

since fibre prestressing was induced through tensile creep, this could be represented by the resulting viscoelastic creep strain, determined quantitatively with a Weibull-based model [29]. Thus, for clarity, the term 'prestrain level' in this paper specifically refers to the viscoelastic creep strain, i.e. the effect of elastic strain is subtracted from the total creep strain in each case. To understand further the underlying mechanisms, recovery force measurements and wide-angle X-ray diffraction (WAXD) were also performed on prestressed fibres, to investigate potential microstructural changes from viscoelastic deformation.

2. Background

2.1 Viscoelastic behaviour

When a polymeric yarn (not constrained by a matrix) is subjected to a constant creep stress, it exhibits responses that are (principally) elastic and viscoelastic. The resulting creep-strain curve may consist of three stages, as shown in Fig. 1(a) [38]. Below the yield creep strain (Stages I and II), the total creep strain $\varepsilon_{\mathrm{ctot}}(t)$ at time t can be represented by a Weibull-based function [39]:

$$\varepsilon_{\mathrm{ctot}}(t) = \varepsilon_{\mathrm{i}} + \varepsilon_{\mathrm{c}}\left[1 - \exp\left(-\left(\frac{t}{\eta_{\mathrm{c}}}\right)^{\beta_{\mathrm{c}}}\right)\right] \tag{1}$$

where ε_{i} is the instantaneous elastic strain from initial application of the stress; the ε_{c} function is the nonlinear time-dependent viscoelastic creep strain, with characteristic life η_{c} and shape parameter β_{c}. Following load removal, the yarn undergoes recovery, as represented by the dashed line in Fig. 1(a) (lower graph), and after elastic recovery, the remaining recovery strain $\varepsilon_{\mathrm{rvis}}(t)$ is [39]:

$$\varepsilon_{\mathrm{rvis}}(t) = \varepsilon_{\mathrm{r}}\left[\exp\left(-\left(\frac{t}{\eta_{\mathrm{r}}}\right)^{\beta_{\mathrm{r}}}\right)\right] + \varepsilon_{\mathrm{f}} \tag{2}$$

where η_{r} and β_{r} are the Weibull parameters, analogous to Eq. (1); ε_{f} is the (non-recoverable) strain resulting from viscous flow. Therefore, to benefit from viscoelastic fibre prestressing, the prestressed polymeric fibres must be moulded into a matrix before the recovery strain eventually decays to its ε_{f} value. Creep and recovery strain-time data from previously published work [29,40] have been utilised for this research. Here, the prestrain level can be represented by $\varepsilon_{\mathrm{c}}(24)$, which is $[\varepsilon_{\mathrm{ctot}}(24\ \mathrm{h}) - \varepsilon_{\mathrm{i}}]$, i.e. the elastic strain is subtracted from the total creep strain at 24 h.

When the prestressed yarn is embedded in a solid matrix or constrained mechanically, a stress will be induced by viscoelastic recovery. Fig. 1(b) represents the stress (i.e. the contraction force relative to yarn cross-sectional area), that can be generated from viscoelastic recovery at a fixed strain. On releasing the creep load at t_{c}, a time window, Δt, is allowed to elapse to enable an initially loose polymeric yarn to contract to a constant strain level, i.e. ε_1. Under these conditions, a time-dependent stress, $\sigma(t)$ can be expected (Fig. 1(b) upper graph, right side), which follows [34]:

$$\sigma(t) = \sigma_{\mathrm{v}}\left[\exp\left(-\left(\frac{\Delta t}{\eta}\right)^{\beta}\right) - \exp\left(-\left(\frac{t}{\eta}\right)^{\beta}\right)\right] \tag{3}$$

where the σ_{v} function represents viscoelastically generated stress, as determined by the characteristic life η and shape β parameters.

2.2 Phase identification of nylon 6,6 fibre

Semi-crystalline nylon 6,6 is usually regarded as a two-phase structural material, consisting of crystalline regions embedded in an amorphous matrix [41,42]. The microstructure of nylon 6,6 has been

intensively studied through wide-angle X-ray diffraction (WAXD) [43-48] and is well understood. It consists of a broad amorphous halo, superimposed with sharp peaks from the crystalline regions [49]. As represented in Fig. 2, for a triclinic Bravais cell structure, three reflections appear when Bragg planes pass through the axes of nearest neighbour chains [42], and the spacings given from (100), (010) and (110) reflections correspond to 4.39 Å, 3.73 Å and 3.66 Å respectively [50]. Usually the latter two reflections join together. Therefore, a unique X-ray fingerprint for nylon 6,6 is obtained. The ideal α-crystal has two strong equatorial diffraction peaks: (i) the (100) peak at 2θ of ~20.3˚, with a distance of ~4.4 Å, corresponds to the inter-chain distance within the hydrogen-bonded sheet; (ii) the joint (010, 110) peak at 2θ of ~23.5˚, with a distance of ~3.7 Å, represents the inter-sheet distance [51,52].

Fig. 3 shows a typical profile analysis of an equatorial diffraction pattern from the semi-crystalline nylon 6,6 fibre used in this work. The normalised area of the crystalline peaks can be used to obtain an absolute degree of crystallinity of the fibre. A relative measure of crystallinity is commonly obtained from [53]:

$$\text{Crystallinity } \% = \frac{A_\text{c} \times 100}{A_\text{c} + A_a} \tag{4}$$

where, A_c and A_a are the integrated areas underneath the crystalline peaks and amorphous halo, respectively.

The diffraction peak width is inversely related to crystallite size. The crystalline reflections from fibres are further broadened by the considerable defects and disorder in the crystal lattice after drawing. Therefore, the 'apparent crystallite size' ACS_{hkl}, rather than actual crystallite size, is produced from profile analysis of equatorial scans using the Scherrer equation [49,53]:

$$ACS_{hkl} = \frac{0.9\lambda}{\Delta\theta_{hkl} \cos\theta_{hkl}} \tag{5}$$

where λ is the X-ray wavelength (angstroms), θ_{hkl} is the peak position of the (*hkl*) crystalline plane (radians), and $\Delta\theta_{hkl}$ is the full-width-half-maximum (*FWHM*) of the (*hkl*) crystalline peak (radians).

Profile analysis can also be used to calculate the index of crystalline perfection (*ICP*), which is based on the shift in crystalline peak position compared to the crystalline features of well-crystallised nylon 6,6 fibre, as first proposed by Bunn and Garner [54]. It is routinely used to monitor small changes in the unit cell volume in chain-axis projection and follows [55]:

$$ICP(\%) = \frac{d_{(100)}/d_{(010,110)} - 1}{0.189} \times 100 \tag{6}$$

where $d_{(100)}$ is the inter-planar spacing of the (100) planes; $d_{(010,\,110)}$ is the inter-planar spacing of the (010, 100) planes; 0.189 is the numerator calculated from a well-crystallised nylon 6,6 structure given by Bunn and Garner [54]. Here, $d_{(100)}$ = 4.4 Å and $d_{(010,\,110)}$ = 3.7 Å are regarded as 'perfect'.

3. Experimental

3.1 Composite sample preparation

Composite sample preparation followed the procedures in previous studies on nylon fibre-based VPPMCs [25-30]. A continuous untwisted multifilament nylon 6,6 yarn (140 filaments, 26 μm filament diameter, 94 tex) supplied by Ogden Fibres Ltd, UK, was used. Annealing of the yarn at 150°C for 0.5 h was required to remove manufacturing-induced residual stresses [26,35], while at least 0.5 h was allowed to elapse for the yarns to acquire equilibrium moisture content before the fibre stretching stage [29]. To produce one batch of composite samples, two similar lengths of annealed nylon yarn were cut, one designated as test, the other being control. The test yarn was subjected to tensile creep, whilst the control

yarn was positioned (unconstrained) in close proximity to ensure the same exposure to ambient conditions (20.0-21.5°C and 30-40% RH). Fig. 4(a) shows a schematic of the experimental setup for fibre prestressing. The test yarn was clamped to the upper and lower bobbins of a bespoke stretching rig (SR); the lower bobbin was fixed to a counterbalanced platform, on which weights could be applied to achieve a specified stress. Here, stress was defined as the load relative to the initial cross-sectional area of the yarn. Thus a range of prestrain levels could be achieved by applying different loads to the rig, and a 24 h time period was adopted for all runs. In this study, three prestrain levels were produced from creep stress values of 330 MPa, 460 MPa and 590 MPa. Following load removal, test and control yarns were cut, folded and brushed into flat ribbons, ready for moulding.

A clear-casting polyester resin, i.e. Reichold Polylite 32032, supplied by MB Fibreglass, UK, was used with 2% MEKP catalyst as the matrix material. A batch of test and control samples was moulded through open-casting, in which two identical aluminium open moulds were used, each with a polished channel of 450 mm length, 10 mm width and 3 mm depth. This enabled the test and control materials to be moulded simultaneously with the same resin mix, so that no differences between the samples would be expected other than effects from the polymeric fibre prestressing process. Moulding was completed within 0.5 h of releasing the creep load and the resin was considered to be sufficiently cured after ~2 h to permit demoulding. Following demoulding, the two composite strips were each cut into five equal lengths, to produce a batch of five test and five control samples, with dimensions of 80 × 10 × 3.2 mm. All samples were held under a weighted steel strip for 24 h to prevent any sample distortion from residual stresses [29]. Samples were then stored in polyethylene bags at room temperature prior to testing. For repeatability, five batches of test and control samples were produced for each prestrain level, corresponding to a total of 50 samples (25 test and 25 control) for each condition. A relatively low fibre volume fraction of 2% was adopted for all composite sample production, as used in previous studies with Charpy impact testing [22,23,25-29,35]; this provided simple fracture patterns and minimised frictional energy losses between the sample and anvil shoulders [27]. Moreover, the high sample transparency facilitated visual inspection during moulding, ensuring problems such as fibre misalignment could be avoided.

3.2 Charpy impact tests

Low velocity impact tests were adopted to evaluate the effect of prestrain level on the impact performance of VPPMCs. These were performed on a Ceast Resil 25 Charpy machine, using a 7.5 Joule hammer at a velocity of 3.8 m/s. To correspond with earlier Charpy-based studies on low V_f nylon 6,6 fibre composite samples [22,23,25-28], a 24 mm span was adopted. Tests were performed two weeks (336 h) after production, and conducted in accordance with the BS EN ISO 179 standard [56]. Since fibres tended to settle towards the bottom of the mould before the matrix had cured, samples were positioned with the fibre-rich side facing away from the pendulum hammer to maximise the effects of prestress on mechanical performance [22].

3.3 Recovery force measurement

The procedures for recovery force measurement followed those previously published [34,57]. A bespoke force measurement rig (FMR) was used [34], with V-slot bobbins that were compatible with the SR as shown in Fig. 4(b). A loop of yarn was annealed, and then attached to the bobbins. Creep was applied with the SR (Fig. 4(a)) following the same procedures described in Section 3.1. Upon load removal, the loop-bobbin assembly was removed from the SR and transferred to the FMR (Fig. 4(b)). The fibre loop was initially in a loose state on the FMR, hence there was no elastic strain component. Within 2-3 min, the loop progressively tightened from viscoelastic recovery, to a fixed strain, which then generated a force (Fig. 1(b)). This contraction force was monitored through voltage output from a transducer located at the top of the FMR. All readings were recorded with ambient conditions of 20.0-21.0˚C and 30-40% RH. Recovery force was monitored up to 1000 h, and two yarn samples at each

stress condition were tested for assessing repeatability. *CurveExpert 1.4* was employed to determine the parameter values for each 24 h creep condition by fitting Eq. (3) to the recovery stress-time results.

3.4 Wide-angle X-ray diffraction (WAXD)

WAXD was adopted to evaluate potential microstructural changes within the nylon 6,6 yarn after fibre stretching. Following load removal, yarns were cut and folded into six parallel lengths, and then brushed into flat ribbons. The fibre ribbons were trimmed to ~100 mm in length, which ensured appropriate fitting into a sample holder. Ribbon width was maintained at ~10 mm which minimised overlapping effects. The flat fibre ribbons were then mounted on WAXD sample holders, and yarns were adjusted to be as parallel as possible.

WAXD scanning was performed with an Empyrean X-ray diffractometer from PANalytical UK Ltd., using Cu-Kα radiation with wavelength λ=1.5406 Å. Detection was provided by a PIXcel^{1D} detector. Wide-angle equatorial scans were performed at 40 kV and 30 mA for a 2θ range of 15-30˚, and the scanning rate was 0.04˚/s. The transmission mode was used with automatic slit settings and the samples could rotate 360˚ in their own plane. Profile analysis was achieved using commercially available software, *MDI Jade 6.0*. The background was maintained as linear. A mathematical model based on the Pearson VII function was adopted, since this offered the best profile fitting to nylon 6 fibre over the Gaussian, Lorentzian and Logistic functions [58]. A shape factor of two ensured adequately stabilised diffraction patterns [48,53,59].

4. Results and discussion

4.1 Effect of creep condition on the impact performance of VPPMCs

The viscoelastic response of the nylon 6,6 fibre in terms of creep and recovery strain has been recently reported [29,40]. Therefore, by utilising the creep parameters from these studies, Eq. (1) was used to determine the prestrain level, $\varepsilon_c(24)$, for each 24 h creep condition. The $\varepsilon_c(24)$ values were found to be 3.39%, 4.03% and 4.82% for the 330 MPa, 460 MPa and 590 MPa creep conditions, respectively. The influence of these creep stress conditions on impact behaviour is shown in Table 1 and Fig. 5. It is clear that the benefit from prestress is greatest at the 460 MPa creep value, giving a 79.2% increase in impact energy absorption compared to control counterparts. Increasing the creep stress further to 590 MPa, reduces the increase to 57.1%, despite the higher prestrain level. Thus an optimum prestrain level exists to maximise the prestress effects for VPPMC production, the greatest increase observed at 460 MPa being verified by one-sided hypothesis testing (5% significance level). Under free viscoelastic recovery strain conditions, the strain-time behaviour of nylon 6,6 fibre shows approximate linear viscoelasticity [40], but this is not directly related to the viscoelastic behaviour of fibres within a VPPMC, since fibres are held under a fixed strain by the matrix. In these cases, viscoelastic energy stored in the fibres is used to generate contraction forces which are transferred to the matrix, as opposed to a physical (lengthwise) contraction of the fibre material. Therefore, the measurement of recovery force at a fixed strain was required to understand further the prestress effect.

4.2 Recovery force

Recovery force outputs, generated from the three creep settings, were monitored up to 1000 h, and results are shown in Fig. 6, in terms of recovery stress. Curve-fits from Eq. (3) are also shown in Fig. 6, and parameter values are listed in Table 2. Since nylon fibre is sensitive to humidity, the spread in data can be attributed to humidity variations, within the limits of environmental control (30-40% RH) [34]. Following load removal, the fibre loops subjected to 460 MPa and 590 MPa show similar recovery rates, but there is divergence beyond ~2 h, the 460 MPa condition producing the greatest force. At 336 h (the age at which Charpy impact tests were performed), the stress from recovery force at each creep condition can be determined from Eq. (3) by using the corresponding parameter values in Table 2. These were

found to be 12.7 MPa, 14.2 MPa and 10.8 MPa for 330 MPa, 460 MPa, and 590 MPa creep conditions, respectively. Effectively, force output from the FMR represents the conditions that may be expected from an ideal matrix (perfectly rigid and stable), in contrast with those from a real VPPMC. Nevertheless, it is clear that the 460 MPa condition, producing the greatest force, corresponds with the observations from Charpy impact testing in Fig. 5.

Since the optimum prestrain level (Section 4.1) is a creep parameter, the strain from subsequent viscoelastic recovery is more appropriate for comparison with recovery stress values in Fig. 6. The decrease in recovery strain, i.e. elapsed strain from t = 0 to 336 h, can be expected to relate directly to the recovery stress at 336 h. By using recovery parameters from previous work [29,40] in Eq. (2), the elapsed recovery strain values were found to be 1.75%, 2.20% and 1.14% for the 330 MPa, 460 MPa and 590 MPa creep conditions respectively. These data show a direct (linear) correlation between elapsed recovery strain and recovery stress; i.e. the mechanisms responsible for force output are synonymous with the expended recovery strain. It is also interesting to note the recovery stress 'efficiency', i.e. the recovery stress results at 336 h relative to their corresponding creep stress values: these are 3.85%, 3.15% and 1.85% at 330 MPa, 460 MPa and 590 MPa, respectively. This indicates a reduction with creep stress (most notably at 590 MPa), suggesting a decrease in mechanical energy storage capability, as discussed in Section 4.5.

4.3 X-ray diffraction

The resulting WAXD patterns of the prestressed fibres are shown in Fig. 7. As facilities were limited to stretching one yarn at a time, there was a 20-68 h range in sample age for the WAXD scanning. Peak positions in Fig. 7 show slight variations, which may be due to variability in sample preparation (as discussed in Section 3.4). There are significant differences in terms of peak intensity from the three creep settings, showing an increase in intensity of both peaks with increasing creep stress. This demonstrates the sensitivity of molecular orientation to the creep loading process.

Further details of peak features were obtained through deconvolution of the diffraction patterns with the profile fitting technique (Section 3.4) and results are listed in Table 3. Also, Fig. 8 highlights the influence of 24 h creep stress values on fibre microstructure in terms of changes in WAXD parameters from Table 3. The amorphous halo position ($2\theta_a$) remains relatively stable with respect to the stress. The increase in crystallinity with creep stress can be attributed to growth in the crystalline phase occurring during the loading process [60]. Although annealed nylon 6,6 fibre was used here, similar increases in crystallinity with applied tensile strains were also observed by Marcellan *et al* [48] on non-annealed nylon 6,6 yarn. Also, they detected a decrease in the reduction of the isotropic amorphous index, and an increase in amorphous orientation. Therefore, the increase in intensity with creep stress (as shown in Fig. 7) can be attributed to orientation occurring in the isotropic amorphous regions.

The index of crystalline perfection, *ICP*, shows an increase with creep stress in Fig. 8. Referring to the spacing data from Table 3, the perpendicular chain-to-chain distance within the $d_{(100)}$ plane increases with creep stress up to 460 MPa, then remains constant at 590 MPa, which is equal to that of the non-annealed yarn [61]. This is also confirmed through apparent crystal size *ACS* data from the as-received fibre in [61]. In contrast, the perpendicular sheet-to-sheet distance $d_{(010,\ 110)}$ decreases with loading, which could be caused by compaction along the *a*-axis direction induced from loading of the molecular chains oriented along the fibre axis. Therefore, it can be inferred that the minimised energy of the structure from annealing [62] is affected by the prestressing process, as the rates of both crystallinity and *ICP* decrease with increasing creep stress (Fig. 8). The inter-chain distance, which is controlled by van der Waals interactions, becomes stabilised between 330 MPa and 460 MPa stress; the inter-sheet distance, controlled by hydrogen bonds, continues to decrease with increasing stress.

4.4 Viscoelastic deformation mechanisms in nylon 6,6 fibre

Nylon 6,6 fibre has demonstrated approximately linear viscoelastic characteristics under low creep deformation levels, i.e. up to ~50 MPa creep stress over a period exceeding 1000 h [63]. Linear

viscoelasticity in this fibre has also been demonstrated under large strain deformation (up to 17% strain) from 330-590 MPa creep stress [40]. This was further verified through time-stress superposition experiments, in that a linear relationship was found between the stress-shift factor and creep stress. While nylon 6,6 fibre is usually regarded as a two-phase system in X-ray diffraction, i.e. crystalline and amorphous regions as discussed in Section 2.2, the amorphous region has been refined into isotropic amorphous and oriented amorphous domains [46,48]. The oriented amorphous regions can be considered as the bridging area that connects the isotropic and crystalline regions, which occurs during the drawing process of the fibre [64]. As in the 'Swiss-cheese' model [65,66], crystals are surrounded by oriented amorphous chains, i.e. taut-tie molecules (TTMs). Thus, viscoelastic deformation within nylon 6,6 can be considered to be controlled by the performance of (i) crystalline regions; (ii) isotropic amorphous regions; and (iii) oriented amorphous domains. Fig. 9 represents a proposed deformation model of nylon 6,6 fibre subjected to tensile creep, demonstrating the increase in crystallinity and molecular orientation.

Generally, for semi-crystalline polymeric fibre, instantaneous elastic deformation is mainly determined by the crystalline regions, while viscoelastic deformation is caused by behaviour within the amorphous regions [67,68]. When nylon 6,6 fibre is subjected to creep conditions, both orientation and phase transformation occur within all three regions (i.e. (i), (ii) and (iii), as designated above). The increase in crystallinity and $ACS_{(100)}$ from creep stress, as shown in Table 3 and Fig. 8, demonstrates growth in the crystalline phase; the increase in intensity is attributed to the increase in orientation with creep stress. Since TTMs are considered to control the mechanical properties of polymeric fibres [48,66], the phase transformation from isotropic amorphous to oriented amorphous ensures the compensation of TTMs through local ordering [69], to provide more potential load carrying molecules when subjected to a higher stress. Following load removal, the full recovery in instantaneous elastic strain infers no creep-induced fracture in (i) [40], while the WAXD parameter values indicate non-recoverable reduction in inter-sheet distances induced by compaction (Section 4.3). Since TTMs are in a highly taut state under creep, the recovery of oriented amorphous regions may dominate the initial recovery stage, i.e. rapid recovery upon load removal. This might explain why, as observed in Fig. 6, the time-dependent recovery stress values generated from the 460 MPa and the 590 MPa creep conditions are notably greater than at 330 MPa for the initial period, below 10 h.

4.5 Viscoelastic prestress mechanisms from fibres within a VPPMC

The viscoelastic deformation of nylon fibre can be represented by a latch-based mechanical model [70], i.e. the time-dependent deformation may be represented by a number of latches, controlled by springs and dashpots, connected in series. During creep loading, the latch elements are progressively triggered to store energy, and a higher applied stress may result in more sites being activated [39]. This correlates with the Charpy impact results as presented in Table 1 (Section 4.1), when 330-460 MPa stress was applied for the 24 h fibre prestressing. Beyond 460 MPa however, although stable linear viscoelasticity was observed [40], there is a decrease in impact benefits from viscoelastic fibre prestressing under 590 MPa stress conditions. This reveals further insights into viscoelastic prestress mechanisms from fibres within a VPPMC.

Referring to the microstructural deformation model as presented in Fig. 9, locations for mechanical energy storage can be considered to consist of elastic energy storage sites (EESTs) and viscoelastic energy storage sites (VESTs). EESTs determine elastic deformation from the crystalline regions, and these are fully recovered immediately after load removal up to the 590 MPa creep stress value [40]; conversely, VESTs control the time-dependent viscoelastic deformation in amorphous regions. Thus, as discussed in Section 4.3, the increase in crystallinity and $ACS_{(100)}$ with applied creep stress values may be considered to correspond with an increase in the number of EESTs, and a reduction in VESTs.

The increase in Charpy impact energy from ~54% to ~79% shows that, although there may be a reduction in the number of VESTs from 330 MPa to 460 MPa, more sites are progressively triggered under the higher creep stress of 460 MPa. When subjected to 590 MPa creep however, since nylon 6,6 fibres are approaching full usage of the energy storage sites under 460 MPa creep, the reduction in

prestress benefits (at 590 MPa) may be caused by: (i) availability of VESTs to store more energy as creep stress increases (a saturation effect) and (ii) VESTs being impeded by interactions caused by increasing molecular orientation (Fig. 7) and possibly crystallographic changes, i.e. $d_{(010,\ 110)}$ and other parameters in Table 3. Thus (i) and (ii) would explain the lower value for viscoelastic recovery stress in Fig. 6 (and elapsed recovery strain) at 590 MPa; also the progressive reduction in recovery stress efficiency with creep stress highlighted in Section 4.2. Therefore, the results suggest there is an optimum prestrain level and consequently applied creep stress condition for VESTs to release the stored energy, to obtain the maximum benefits from viscoelastic fibre prestressing within a VPPMC.

5. Conclusions

To understand further the viscoelastic deformation and prestress mechanisms from nylon 6,6 fibres within a VPPMC, we investigated the effects of creep stress magnitude on impact performance in this work. Recovery force measurement and WAXD were used to provide further insights at the microstructural level. The main findings are:

(i) The creep stress applied to fibres for VPPMC production can be quantitatively represented by the resulting viscoelastic creep strain. Charpy impact test results show a limitation in mechanical benefits from prestress effects, when fibres are subjected to the highest creep value, i.e. 590 MPa for 24 h. We suggest that an optimum applied creep condition exists to maximise the prestress benefits for VPPMC production; this is verified by recovery force measurements in that, the (intermediate) 460 MPa 24 h creep condition gives the highest recovery force beyond ~2 h.

(ii) Findings from WAXD patterns show that crystallinity increases with fibre creep stress. The deformation in crystalline regions is non-recoverable, i.e. an offset in crystalline spacing is observed; the degree of orientation is also increased.

(iii) By considering both the three-phase microstructural model and latch-based mechanical model, a viscoelastic prestress mechanism is proposed. It offers an explanation to the observation that there is an optimum creep stress level to maximise the prestress benefits generated by the fibres in a VPPMC.

Charpy impact results demonstrate the effect of applied creep stress on the mechanical performance of VPPMCs. Since the mechanical improvements from viscoelastically generated prestress are limited by the viscoelastic creep strain produced in the fibres, further optimisation of load-time conditions to produce VPPMCs could be considered to maximise the prestress effect. Clearly, this would benefit the potential exploitation of VPPMCs for industrial applications.

Acknowledgements

Financial support from the China Scholarship Council and the School of Engineering & Computer Science (PhD degree fee waiver) for B.W. is gratefully acknowledged. Special thanks go to Garry Robinson from the School of Engineering & Computer Science and Dr M Grazia Francesconi from the School of Mathematics & Physical Sciences at the University of Hull, for their technical support.

References

[1] Benedikt B, Kumosa M, Predecki PK, Kumosa L, Castelli MG, Sutter JK. An analysis of residual thermal stresses in a unidirectional graphite/PMR-15 composite based on X-ray diffraction measurements. Compos Sci Technol 2001;61(14):1977-94.

[2] Parlevliet PP, Bersee HE, Beukers A. Residual stresses in thermoplastic composites - a study of the literature. Part I: Formation of residual stresses. Compos Part A-Appl Sci Manuf 2006;37(11):1847-57.

[3] Hull D, Clyne T. An introduction to composite materials. Cambridge University Press, Cambridge, 1996.

[4] Parlevliet PP, Bersee HE, Beukers A. Residual stresses in thermoplastic composites - a study of the literature. Part III: Effects of thermal residual stresses. Compos Part A-Appl Sci Manuf 2007;38(6):1581-96.

[5] Tuttle ME, Koehler RT, Keren D. Controlling thermal stresses in composites by means of fiber prestress. J Compos Mater 1996;30(4):486-502.

[6] Zhigun IG. Experimental evaluation of the effect of prestressing the fibers in two directions on certain elastic characteristic of woven-glass reinforced plastics. Mech Compos Mater 1968;4(4-6):691-5.

[7] Tuttle ME. A mechanical/thermal analysis of prestressed composite laminates. J Compos Mater 1988;22(8):780-92.

[8] Schulte K, Marissen R. Influence of artificial pre-stressing during curing of CFRP laminates on interfibre transverse cracking. Compos Sci Technol 1992;44(4):361-7.

[9] Sui GX, Yao G, Zhou BL. Influence of artificial pre-stressing during the curing of VIRALL on its mechanical properties. Compos Sci Technol 1995;53(4):361-4.

[10] Zhao J, Cameron J. Polypropylene matrix composites reinforced with pre-stressed glass fibers. Polym Compos 1998;19(3):218-24.

[11] Motahhari S, Cameron J. Impact strength of fiber pre-stressed composites. J Reinf Plast Comp 1998;17(2):123-30.

[12] Hadi AS, Ashton JN. On the influence of pre-stress on the mechanical properties of a unidirectional GRE composite. Compos Struct 1998;40(3-4):305-11.

[13] Motahhari S, Cameron J. Fibre prestressed composites: improvement of flexural properties through fibre prestressing. J Reinf Plast Comp 1999;18(3):279-88.

[14] Dvorak GJ, Suvorov AP. The effect of fiber pre-stress on residual stresses and the onset of damage in symmetric laminates. Compos Sci Technol 2000;60(8):1129-39.

[15] Jevons MP. The effects of fibre pre-stressing on the impact performance of composite laminates. PhD Thesis, United Kingdom, Cranfield University 2004.

[16] Krishnamurthy S. Pre-stressed advanced fibre reinforced composites fabrication and mechanical performance. PhD Thesis, United Kingdom, Cranfield University 2006.

[17] Bekampienė P, Domskienė J, Širvaitienė A. The effect of pre-tension on deformation behaviour of natural fabric reinforced composite. Mater Sci 2011;17(1):56-61.

[18] Širvaitienė A, Jankauskaitė V, Bekampienė P, Norkaitis J. Vegetable fiber pre-tensioning influence on the composites reinforcement. Polym Compos 2013;34(9):1533-7.

[19] Nishi Y, Okada T, Okada S, Hirano M, Matsuda M, Matsuo A, Faudree MC. Effects of tensile prestress level on impact value of 50 vol% continuous unidirectional 0 degree oriented carbon fiber reinforced epoxy polymer (CFRP). Mater Trans 2014;55(2):318-22.

[20] Mostafa NH, Ismarrubie ZN, Sapuan SM, Sultan MTH. The influence of equi-biaxially fabric prestressing on the flexural performance of woven E-glass/polyester-reinforced composites. J Compos Mater 2015;50(24):3385-3393.

[21] Mostafa NH, Ismarrubie ZN, Sapuan SM, Sultan MTH. Effect of equi-biaxially fabric prestressing on the tensile performance of woven E-glass/polyester reinforced composites. J Reinf Plast Comp 2016;35(14):1093-103.

[22] Fancey KS. Investigation into the feasibility of viscoelastically generated pre-stress in polymeric matrix composites. Mat Sci Eng A-Struct 2000;279(1-2):36-41.

[23] Fancey KS. Prestressed polymeric composites produced by viscoelastically strained nylon 6,6 fibre reinforcement. J Reinf Plast Comp 2000;19(15):1251-66.

[24] Pang JWC, Fancey KS. Analysis of the tensile behaviour of viscoelastically prestressed polymeric matrix composites. Compos Sci Technol 2008;68(7-8):1903-10.

[25] Fancey KS. Fiber-reinforced polymeric composites with viscoelastically induced prestress. J Adv Mater 2005;37(2):21-9.

[26] Fancey KS. Viscoelastically prestressed polymeric matrix composites - potential for useful life and impact protection. Compos Part B-Eng 2010;41(6):454-61.

[27] Fazal A, Fancey KS. Viscoelastically prestressed polymeric matrix composites - Effects of test span and fibre volume fraction on Charpy impact characteristics. Compos Part B-Eng 2013;44(1):472-9.

[28] Fancey KS, Fazal A. Prestressed polymeric matrix composites: longevity aspects. Polym Compos 2015;37(7):2092-7.

[29] Wang B, Fancey KS. Towards optimisation of load-time conditions for producing viscoelastically prestressed polymeric matrix composites. Compos Part B-Eng 2016;87:336-42.

[30] Pang JWC, Fancey KS. The flexural stiffness characteristics of viscoelastically prestressed polymeric matrix composites. Compos Part A-Appl Sci Manuf 2009;40(6-7):784-90.

[31] Fazal A, Fancey KS. Performance enhancement of nylon/Kevlar fiber composites through viscoelastically generated pre-stress. Polym Compos 2014;35:931-8.

[32] Fancey KS. Viscoelastically prestressed polymeric matrix composites: An overview. J Reinf Plast Comp 2016;35(17):1290-301.

[33] Daynes S, Diaconu CG, Potter KD, Weaver PM. Bistable prestressed symmetric laminates. J Compos Mater 2010;44(9):1119-37.

[34] Pang JWC, Lamin BM, Fancey KS. Force measurement from viscoelastically recovering Nylon 6,6 fibres. Mater Lett 2008;62(10-11):1693-6.

[35] Pang JWC, Fancey KS. An investigation into the long-term viscoelastic recovery of Nylon 6,6 fibres through accelerated ageing. Mat Sci Eng A-Struct 2006;431(1-2):100-5.

[36] Wang B, Fancey KS. A bistable morphing composite using viscoelastically generated prestress. Mater Lett 2015;158:108-10.

[37] Wang B, Ge C, Fancey KS. Snap-through behaviour of a bistable structure based on viscoelastically generated prestress. Compos Part B-Eng 2017;114:23-33.

[38] Lakes RS. Viscoelastic solids, CRC Press, Washington 1998.

[39] Fancey KS. A latch-based Weibull model for polymeric creep and recovery. J Polym Eng 2001;21(6):489-509.

[40] Wang B, Fancey KS. Application of time-stress superposition to viscoelastic behavior of polyamide 6,6 fiber and its 'true' elastic modulus. J Appl Polym Sci 2017;134(24):1-9.

[41] Lin DJ, Chang CL, Lee CK, Cheng LP. Fine structure and crystallinity of porous Nylon 66 membranes prepared by phase inversion in the water/formic acid/Nylon 66 system. Eur Polym J 2006;42(2):356-67.

[42] Segerman E, Stern P. Two-phase model for structure of polymers. Nature 1966;210:1258-9.

[43] Dumbleton J, Buchanan D, Bowles B. Characterization of nylon 66 structure from x-ray diffraction. J Appl Polym Sci 1968;12(9):2067-78.

[44] Hsiao BS, Barton R, Quintana J. Simple on-line X-ray setup to monitor structural changes during fiber processing. J Appl Polym Sci 1996;62(12):2061-8.

[45] Starkweather HW, Whitney JF, Johnson DR. Crystalline order in nylon 66. J Polym Sci Polym Chem 1963;1(2):715-23.

[46] Marcellan A, Bunsell AR, Piques R, Colomban P. Micro-mechanisms, mechanical behaviour and probabilistic fracture analysis of PA 66 fibres. J Mater Sci 2003;38(10):2117-41.

[47] Feldman AY, Wachtel E, Vaughan GBM, Weinberg A, Marom G. The brill transition in transcrystalline nylon-66. Macromolecules 2006;39(13):4455-9.

[48] Marcellan A, Bunsell AR, Laiarinandrasana L, Piques R. A multi-scale analysis of the microstructure and the tensile mechanical behaviour of polyamide 66 fibre. Polymer 2006;47(1):367-78.

[49] Kohan MI. Nylon plastics handbook, vol. 378, Hanser, Munich 1995.

[50] Lu Y, Zhang Y, Zhang G, Yang M, Yan S, Shen D. Influence of thermal processing on the perfection of crystals in polyamide 66 and polyamide 66/clay nanocomposites. Polymer 2004;45(26):8999-9009.

[51] Suzuki A, Chen Y, Kunugi T. Application of a continuous zone-drawing method to nylon 66 fibres. Polymer 1998;39(22):5335-41.

[52] Navarro-Pardo F, Martínez-Barrera G, Martínez-Hernández AL, Castaño VM, Rivera-Armenta JL, Medellín-Rodríguez F, Velasco-Santos C. Effects on the thermo-mechanical and crystallinity properties of nylon 6, 6 electrospun fibres reinforced with one dimensional (1D) and two dimensional (2D) carbon. Materials 2013;6(8):3494-513.

[53] Lewin M. Handbook of fiber chemistry, CRC Press, New York 2006.

[54] Bunn CW, Garner EV. The crystal structures of two polyamides ('nylons'). P Roy Soc A-Math Phy 11947;89(1016):39-68.

[55] Dismore PF, Statton WO. Chain folding in oriented nylon 66 fibers. J Polym Sci Polym Symp 1966;13(1):133-48.

[56] BS EN ISO 179-1. Plastics-determination of Charpy impact properties-Part 1: non-instrumented impact test. European Committee for Standardization, Bruxelles 2010.

[57] Fazal A, Fancey KS. Viscoelastically generated prestress from ultra-high molecular weight polyethylene fibres. J Mater Sci 2013;48(16):5559-70.

[58] Heuvel H, Huisman R, Lind K. Quantitative information from X-ray diffraction of nylon-6 yarns. I. Development of a model for the analytical description of equatorial X-ray profiles. J Polym Sci Polym Phys 1976;14(5):921-40.

[59] Murthy NS, Bray RG, Correale ST, Moore RAF. Drawing and annealing of nylon-6 fibres: studies of crystal growth, orientation of amorphous and crystalline domains and their influence on properties. Polymer 1995;36(20):3863-73.

[60] Murthy NS. Metastable crystalline phases in nylon 6. Polym Commun 1991;32(10):301-5.

[61] Wang B. Viscoelastically prestressed composites: towards process optimisation and application to morphing structures. PhD Thesis, United Kingdom, University of Hull 2016.

[62] Matsuoka S. Structural relationship between thermomechanical history and strength of polymeric solids. Polym Eng Sci 1974;14(3):162-6.

[63] Howard WH, Williams ML. The viscoelastic properties of oriented nylon 66 fibers: Part I: creep at low loads and anhydrous conditions. Text Res J 1963;33(9):689-96.

[64] Peterlin A. Drawing and annealing of fibrous material. J Appl Phys 1977;48(10):4099-108.

[65] Prevorsek DC, Harget PJ, Sharma RK, Reimschuessel AC. Nylon 6 fibers: changes in structure between moderate and high draw ratios. J Macromol Sci B 1973;8(1-2):127-56.

[66] Bukošek V, Prevoršek DC. Model of nylon 6 fibers microstructure microfibrillar model or “Swiss-Cheese” model? Int J Polym Mater Po 2000;47(4):569-592.

[67] Starkova O, Yang J, Zhang Z. Application of time-stress superposition to nonlinear creep of polyamide 66 filled with nanoparticles of various sizes. Compos Sci Technol 2007;67(13):2691-8.

[68] Bower AF. Applied mechanics of solids, CRC Press, New York 2009.

[69] Statton W. High-temperature annealing of drawn nylon 66 fibers. J Polym Sci Polym Phys 1972;10(8):1587-92.

[70] Fancey KS. A mechanical model for creep, recovery and stress relaxation in polymeric materials. J Mater Sci 2005;40(18):4827-31.

Table 1

Charpy impact test results from each 24 h creep condition. Samples were tested 336 h after moulding. Five batches of samples were tested for each prestressing condition (5 test and 5 control samples in each batch); SE is the standard error.

Batch	Mean impact energy (kJ m^{-2})		Increase in energy (%)
	Test ± SE	Control ± SE	
330 MPa (24 h)	33.93 ± 3.14	23.78 ± 1.48	42.64
	37.02 ± 1.78	20.71 ± 0.63	78.76
	35.36 ± 1.71	25.03 ± 0.96	41.26
	36.71 ± 2.89	25.60 ± 1.15	43.37
	35.58 ± 1.96	21.61 ± 1.13	64.69
Mean ± SE	35.7 ± 1.0	23.4 ± 0.6	54.1 ± 7.5
460 MPa (24 h)	39.63 ± 2.22	24.08 ± 0.74	64.60
	37.30 ± 0.54	22.28 ± 0.88	67.39
	38.57 ± 1.35	19.46 ± 0.15	98.21
	39.36 ± 0.95	22.59 ± 0.66	74.23
	44.81 ± 1.86	23.41 ± 0.59	91.36
Mean ± SE	39.9 ± 0.8	22.4 ± 0.4	79.2 ± 6.7
590 MPa (24 h)	30.08 ± 2.51	21.49 ± 1.25	39.96
	35.77 ± 1.46	21.72 ± 0.44	64.70
	35.62 ± 1.11	22.19 ± 0.63	60.48
	37.64 ± 1.75	23.98 ± 0.82	56.93
	36.59 ± 1.36	24.29 ± 0.37	63.51
Mean ± SE	35.1 ± 0.6	22.7 ± 0.3	57.1 ± 4.5

Table 2

Recovery stress parameter values determined by fitting Eq. (3) to the experimental data in Fig. 6; *r* is the correlation coefficient.

24 h applied stress (MPa)	Recovery stress parameters				
	σ_v (MPa)	Δt (h)	η (h)	β	*r*
330	16.92	0.094	69.21	0.3699	0.9967
460	63.35	0.065	3.78	0.0720	0.9963
590	241.3	0.053	0.13	0.0139	0.9909

Table 3

Microstructural parameters for the prestressed nylon 6,6 fibre.

	Sample	0 MPa	330 MPa (24 h)	460 MPa (24 h)	590 MPa (24 h)
(100)	2θ (˚)	20.52	20.37	20.34	20.34
	d (Å)	4.341	4.372	4.378	4.378
	FWHM	1.41	1.36	1.32	1.31
	ACS (Å)	57	59	61	62
(010, 110)	2θ (˚)	23.55	23.44	23.58	23.58
	d (Å)	3.817	3.813	3.812	3.809
	FWHM	2.10	1.92	2.09	2.04
	ACS (Å)	39	42	39	40
Amorphous	2θ (˚)	22.77	22.78	22.64	22.69
	FWHM	3.52	3.88	3.67	3.70
Crystallinity (%)		52.97	58.15	59.95	60.34
ICP (%)		72.6	77.6	78.5	79.1

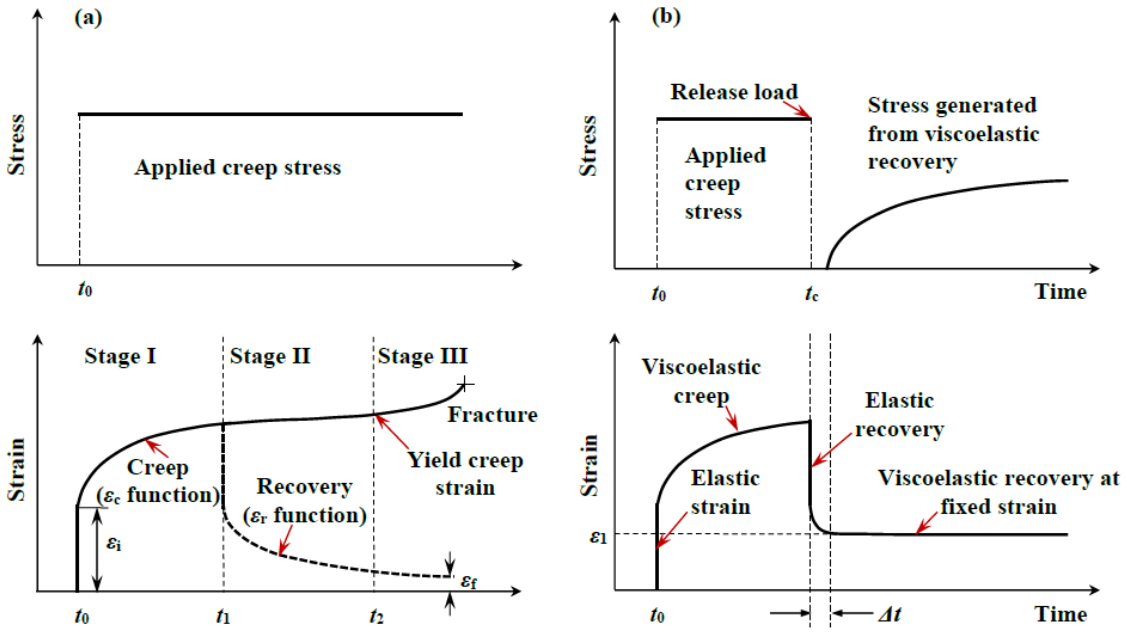

Fig. 1. Schematic of the creep and recovery characteristics of a polymeric yarn: (a) creep and recovery behaviour under a constant stress; (b) creep and recovery cycle following load removal at t_c, and subsequent recovery stress (contraction force relative to yarn cross-sectional area) at a fixed strain, ε_1.

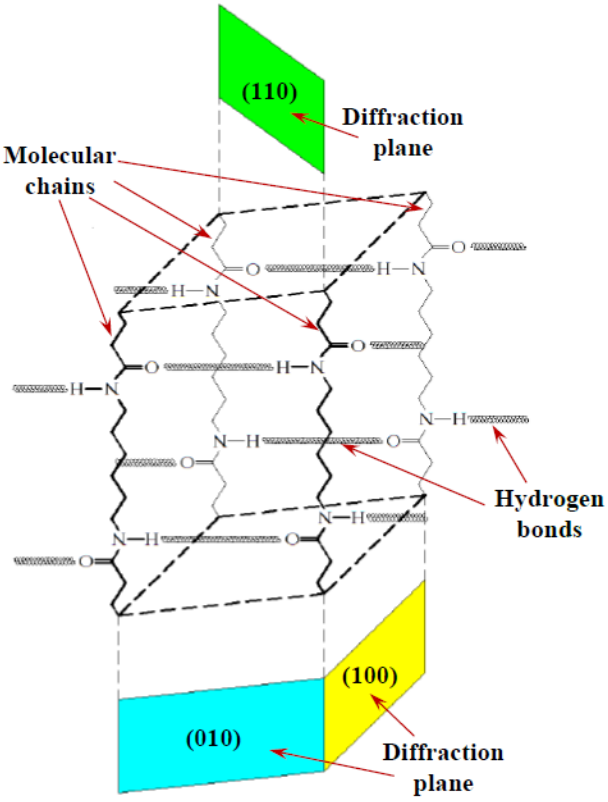

Fig. 2. Example schematic representation of the α-form molecular unit cell structure in nylon 6,6 fibre, showing the associated diffractional crystalline planes.

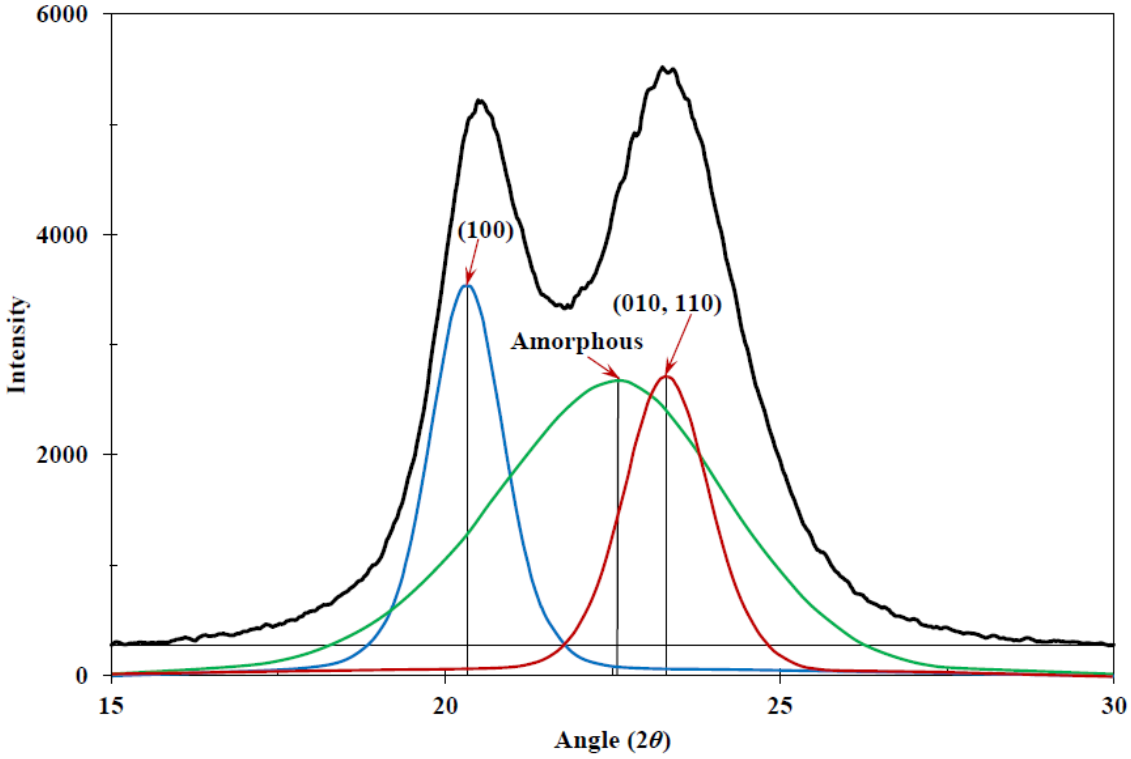

Fig. 3. Example of profile analysis of an equatorial diffraction pattern from nylon 6,6 fibre used in this work.

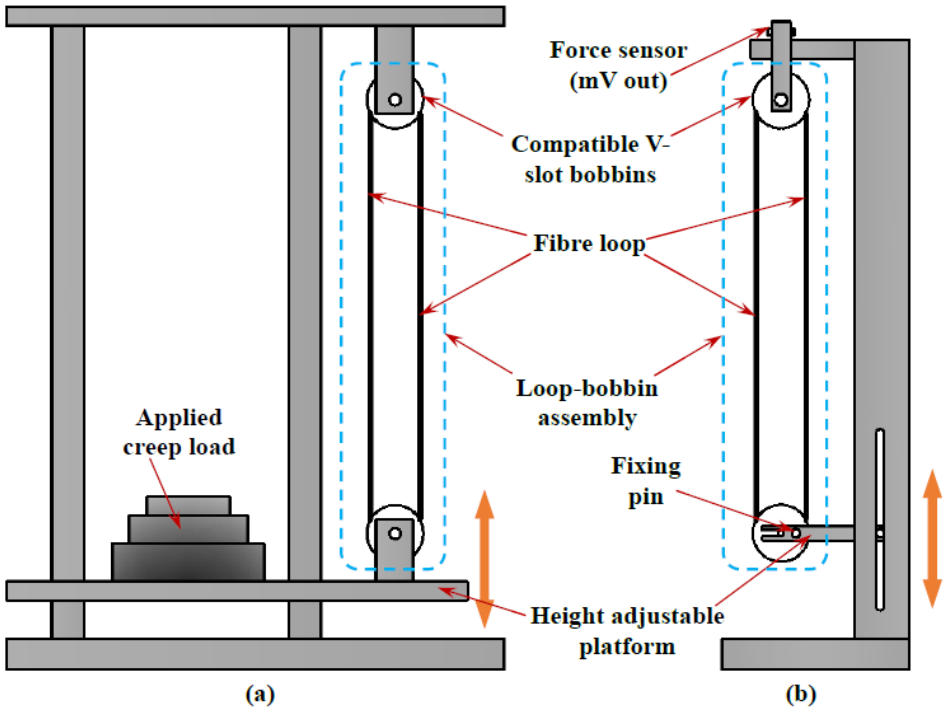

Fig. 4. Schematic representation of (a) the bespoke stretching rig for fibre prestressing and (b) the recovery force measurement rig.

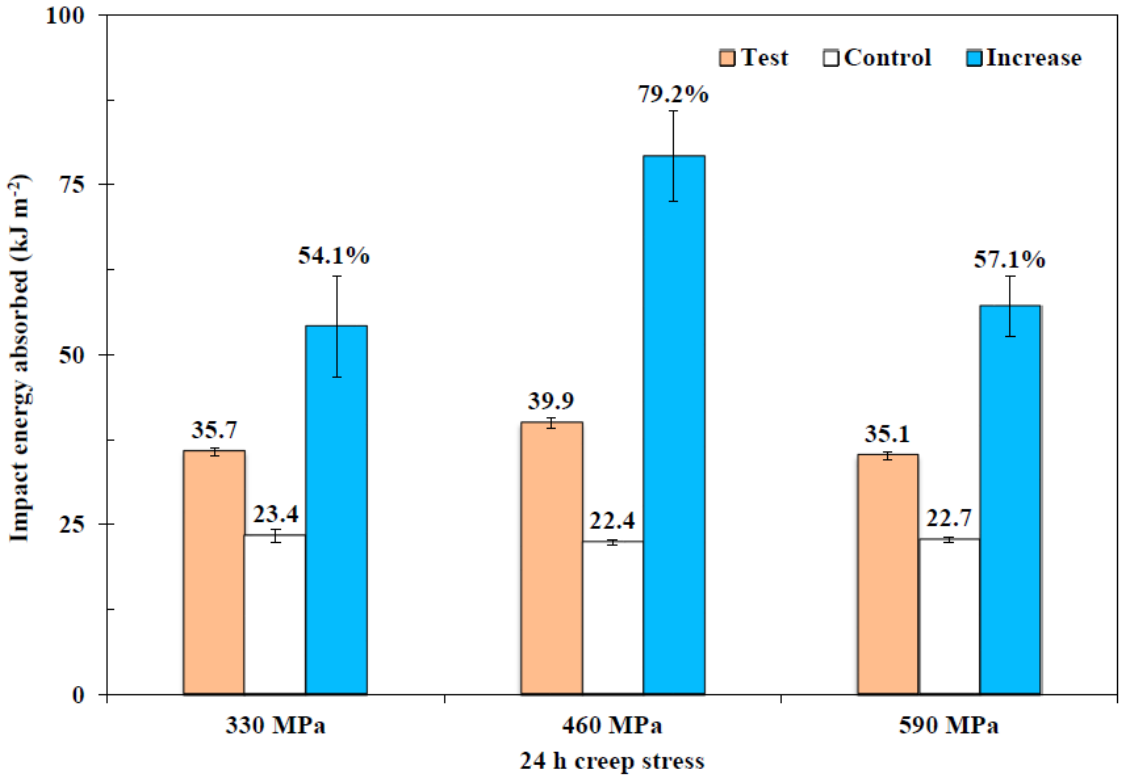

Fig. 5. Charpy impact test results from Table 1; error bars represent the standard error.

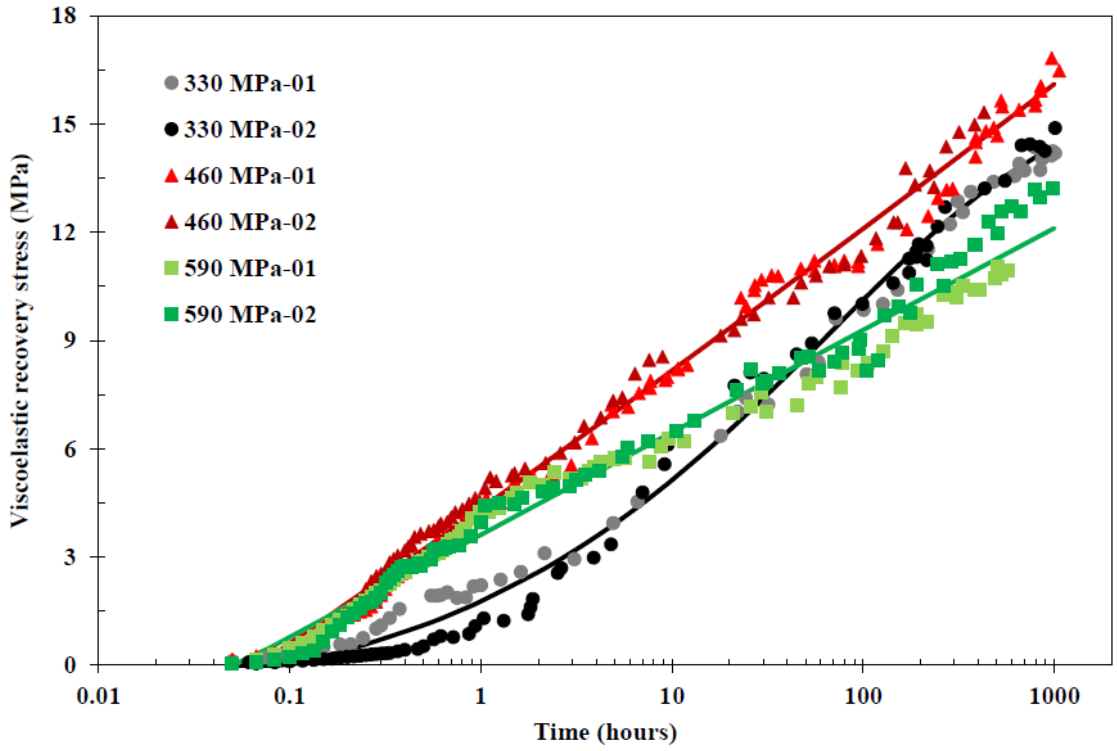

Fig. 6. Measured viscoelastic recovery stress generated from the three 24 h creep conditions with curve-fits from Eq. (3).

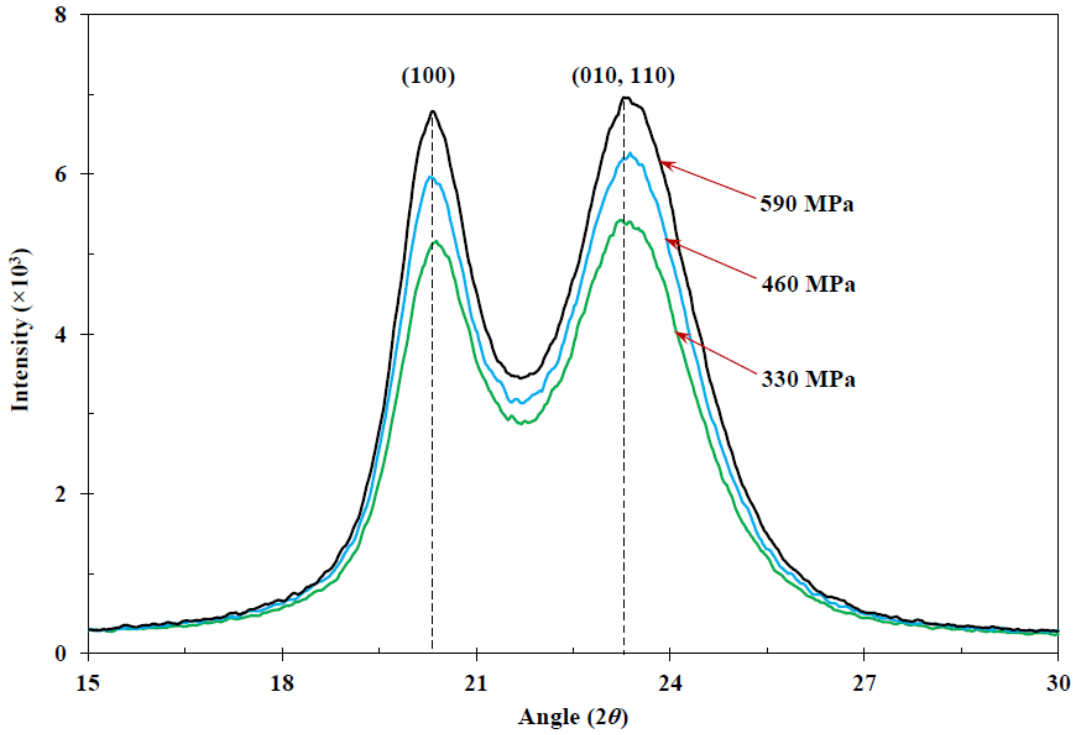

Fig. 7. Comparison of WAXD patterns for the nylon 6,6 fibre under the three 24 h creep conditions. Sample age (following load removal) was 20 h for 330 MPa, 44 h for 460 MPa and 68 h for 590 MPa.

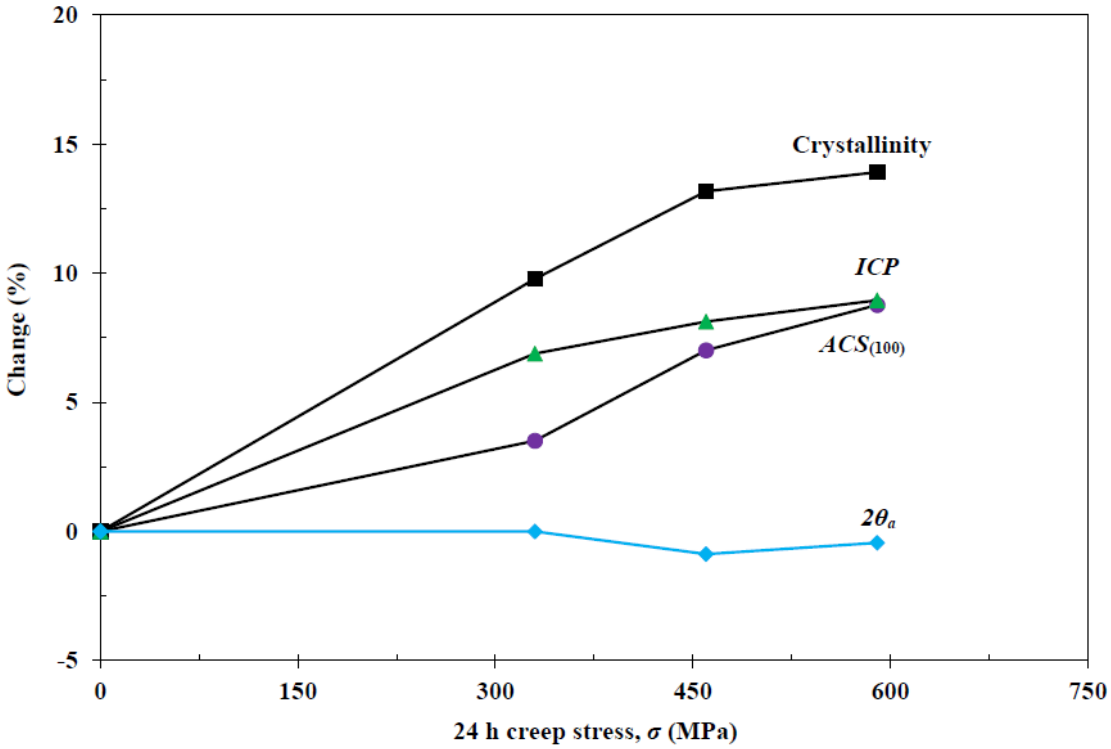

Fig. 8. Changes in microstructural parameters with creep stress in terms of crystallinity, apparent crystal size (*ACS*), index of crystalline perfection (*ICP*) and amorphous peak position ($2\theta_a$).

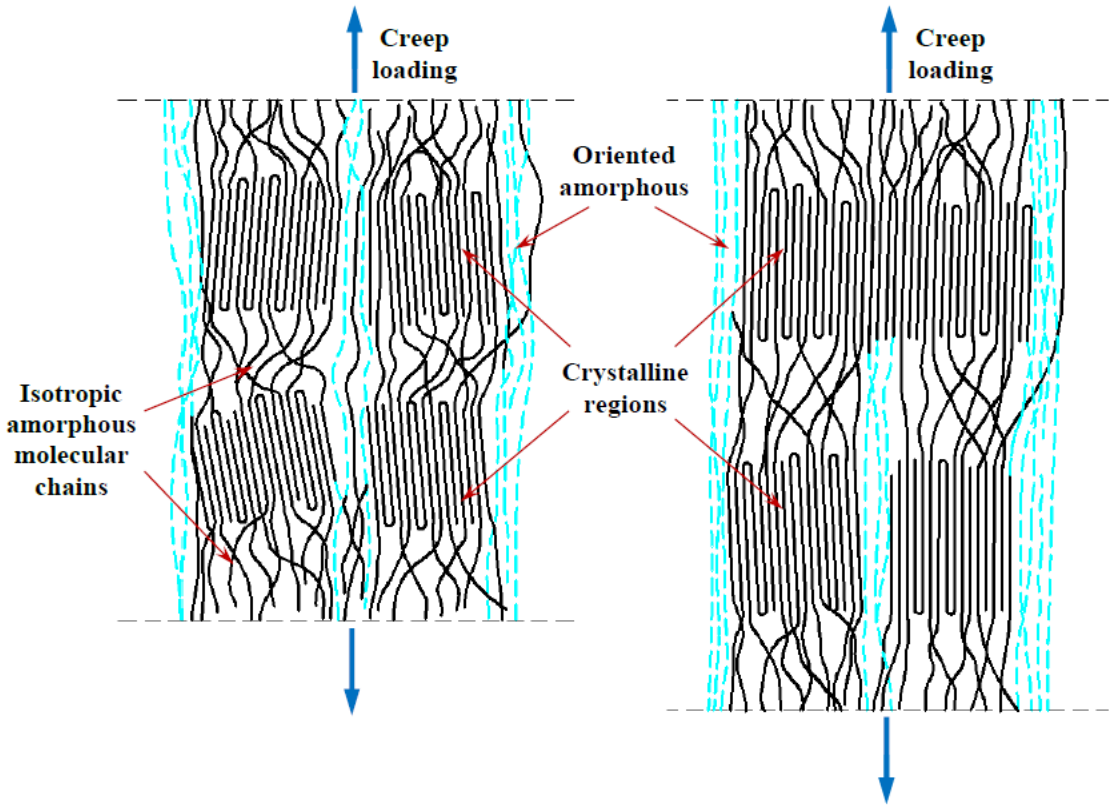

Fig. 9. Schematic representation of creep deformation within nylon 6,6 fibre, demonstrating the increase in crystallinity and molecular orientation. Solid lines in crystalline regions represent both molecular chains and sheets; dashed lines represent taut-tie molecules.